JOURNAL OF MATERIALS SCIENCE **39** (2004) 6311–6323

Preparation of tricalcium phosphate/alumina composite nanoparticles and self-reinforcing composites by simultaneous precipitation

Y. X. PANG, X. BAO*, L. WENG
Institute of Polymer Technology and Materials Engineering, Loughborough University, Loughborough, Leicestershire LE11 3TU, UK
E-mail: x.bao@lboro.ac.uk

The composite nanoparticles and corresponding self-reinforcing composites comprising tricalcium phosphate (TCP) and alumina (Al_2O_3) were synthesized by simultaneous precipitation from the $CaCl_2$, $AlCl_3$ and $(NH_4)_2HPO_4$ aqueous solutions, using aqueous NH_4OH as precipitant. Influences of the precipitating media pH and the Ca/P atomic ratios on phase composition and morphology of the composites were investigated. Results showed that except for the major phases β-TCP and α-Al_2O_3, there was always a third minor phase in the calcined composites coprecipitated either in neutral or alkaline condition. Formation of β-TCP is, however, favored at pH 9.2, whereas more of the third phase, mainly $AlPO_4$, is formed under neutral condition. High Ca/P ratios suppress the formation of α-Al_2O_3 phase under alkaline precipitating condition, but the effect is less significant in neutral condition. TEM observation showed that the 'as prepared' composite particles are nano-sized but interconnected to form a network-like morphology. They were changed to a core-shell-like structure after calcination, while their nano-scale dimension was retained. FEGSEM analysis revealed that the α-Al_2O_3 phase in the sintered composite compacts was in the form of fibrils dispersed in the phosphate phases. These *in situ* formed fibrils impart a unique role in self-reinforcement of the sintered composites. Mechanical measurements showed that the incorporation of alumina reinforced β-TCP effectively: the flexural strength increased from 15 MPa of the pure β-TCP to 84 MPa of the composite with 40 wt% of α-Al_2O_3.

1. Introduction

The β-form tricalcium phosphate (β-TCP) is one of the most attractive bioceramics due to its promising bioactivity and biocompatibility and is widely used in medicine and dentistry [1]. For instance, porous β-TCP was developed as a carrier for an implantable controlled drug delivery system for the local antibiotic treatment of bone infections [2]. The β-TCP dental cement with controlled release of antimicrobial agents has been used for the treatment of carious dentine [3]. However, the most attractive potential of β-TCP is for repairing hard tissues of vertebrates, such as human body [4, 5]. Ito *et al.* [6] reported that a small amount of zinc-doped β-TCP showed high cytocompatibility and proliferation of osteoblastic MC3T3-E1 cells was significantly increased on the composite ceramic, compared with those without zinc. Recently, the biphasic bioceramics comprising β-TCP and hydroxyapatite (HA) have drawn much attention as an ideal bone substitute [7–9]. The high bioactivity retains in the biphasic material, while the incorporation of β-TCP provides well-controllable biodegradability, which can be achieved simply by adjustment of the phase composition [1].

The major shortcoming for β-TCP, like HA or the biphasic ceramics, is its poor mechanical strength. Blending these bioceramics with other mechanically strong ceramics is a usual way to improve their mechanical strength. Some researches have been reported, but most of them were concentrated on HA such as HA/zirconia [10], HA/alumina [11] composites. Unfortunately, the additives usually induce HA transformation into β-TCP at high temperature, or even react with it, leading to the loss of bioactive phase [12]. It is known that the thermal stability of β-TCP is superior to HA and other apatites. This provides an advantage for making composites with other ceramics in respect of improving the mechanical properties. The β-TCP/TiO_2 composite with dense titania core, prepared by slip casting, was found to have cytocompatibility and potential medical application [13]. The β-TCP/glass composite was reported to be of relatively high fracture toughness and bending strength [14]. Yamashita *et al.* [15] reported

*Author to whom all correspondence should be addressed.

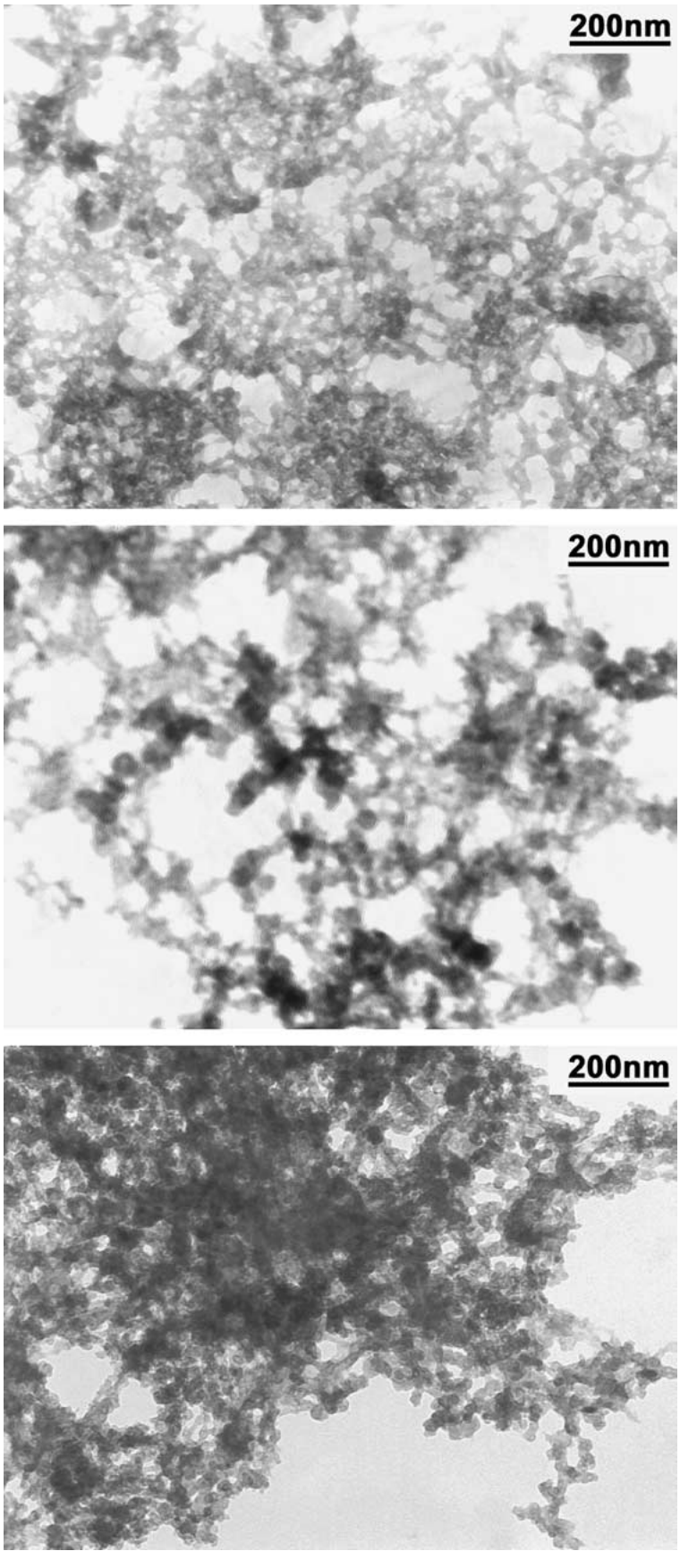

Figure 1 TEM micrographs for the 'as prepared' composites coprecipitated at pH = 7.0 Ca/P molar ratios: 1.45 (top), 1.50 (middle) and 1.60 (bottom).

the preparation of multilayered TCP/Al_2O_3 composite by electrophoretic processing. More recently, Jun *et al.* [16] fabricated TCP-coated porous Al_2O_3 for implant in consideration of improving mechanical strength.

Aluminum oxide (Al_2O_3) is of excellent bio-inertness and very good mechanical properties [11, 17]. The incorporation of Al_2O_3 into β-TCP leads to improved mechanical strength while retains the

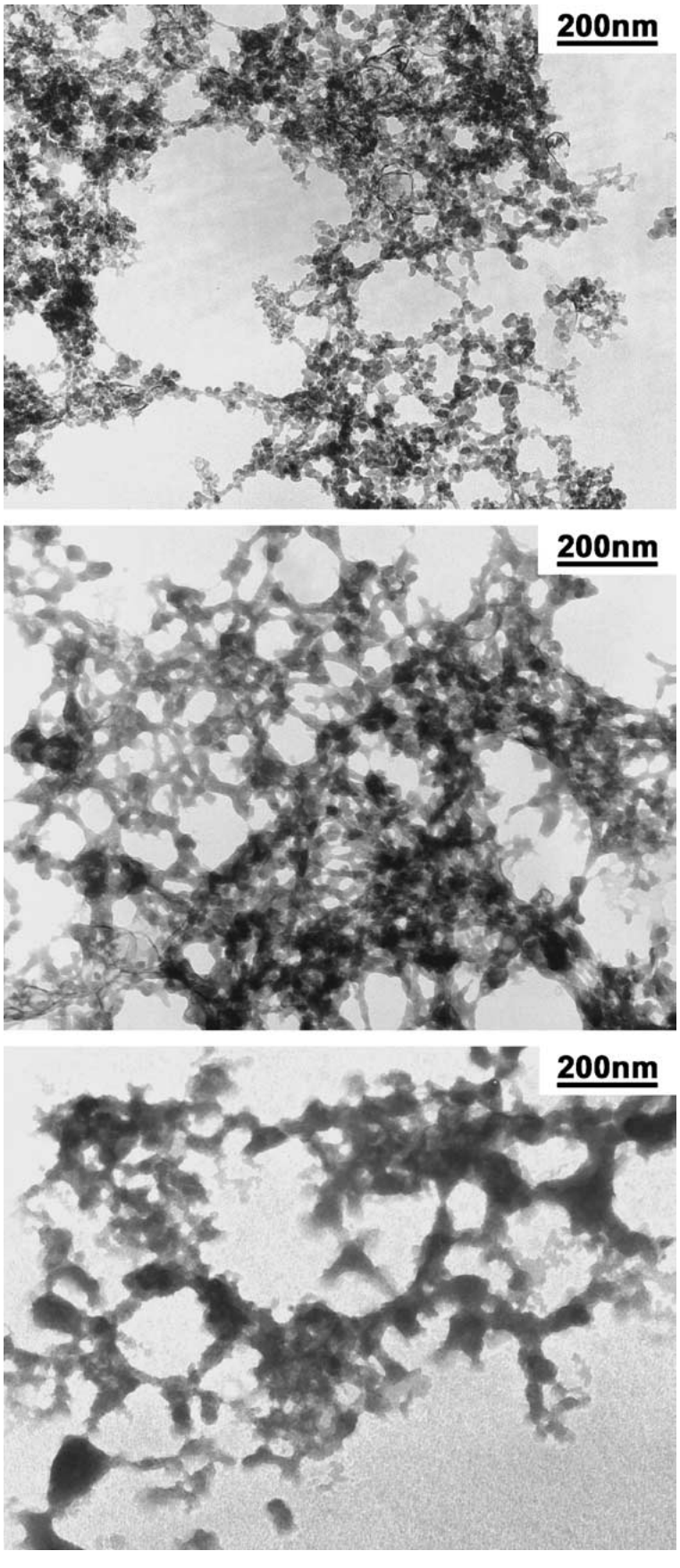

Figure 2 TEM micrographs for the 'as prepared' composites coprecipitated at pH = 9.2 Ca/P molar ratios: 1.45 (top), 1.50 (middle) and 1.60 (bottom).

bioactivity, as reported by the references cited above. In this paper, a wet chemistry route, simultaneous precipitation, was employed to *in situ* prepare TCP/Al_2O_3 composite nanoparticles and self-reinforcing composites from them. This method is simple and flexible, compared with electrophoretic processing [15] or dip coating [16]. Most importantly, the synthesized nanocomposite precipitates can be converted to self-

reinforcing composites by *in situ* formation of Al_2O_3 fibrils during sintering. This is different from the direct powder blending [11]. There were no Al_2O_3 fibrils used in the composites and the current report is the first example of fabricating self-reinforcing ceramic composites based on the best of our knowledge.

2. Materials and methods

2.1. Synthesis

Aluminium chloride hexahydrate (Fisher Scientific, UK) and calcium chloride (Aldrich) 0.5 M aqueous solutions were mixed in the amounts to form predetermined TCP-to-Al_2O_3 ratios. Ammonium hydrogen phosphate (Aldrich) 0.3 M aqueous solution was then added under vigorous stirring. The precipitates were formed immediately. The pH values of the reacting systems were set at 7.0 and 9.2 by loading proper amount of ammonium hydroxide solution (Aldrich). After the system was kept stirring at room temperature for 24 h, the precipitates were reclaimed by centrifugation and then washed with water. Five cycles of washing and centrifuging were performed to ensure the removal of ammonium chloride. Distilled water was used throughout the experiments.

2.2. Mechanical test

The three-point bending tests of the composites were carried out on a Lloyds tensile tester, according to the British Standard BS EN 638–3. The span was set at 24 mm and the bending rate at 0.5 mm/min. At least three beams were tested for each sample and the average was reported. Sample beams were prepared as follows: The composite powders were first calcined at 800°C for 6 h and slightly ground in an agate mortar, and then

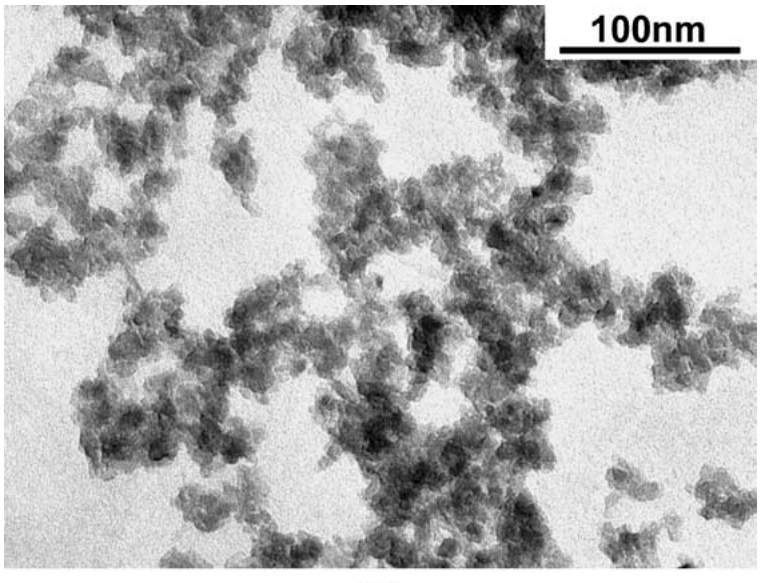

(a)

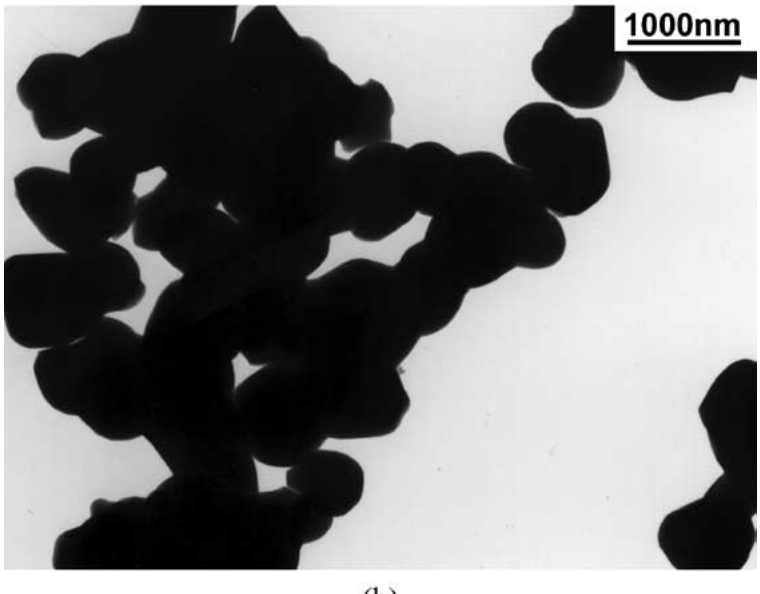

(b)

Figure 3 Particle morphology of the neat Al_2O_3, TCP and composite nanoparticles of TCP/Al_2O_3 = 60/40 by mass after calcination at 900°C for 6 h: (a) neat Al_2O_3, (b) neat TCP, (c) composite nanoparticles prepared at pH = 7.0, and (d) composite nanoparticles prepared at pH = 9.2. (*Continued*)

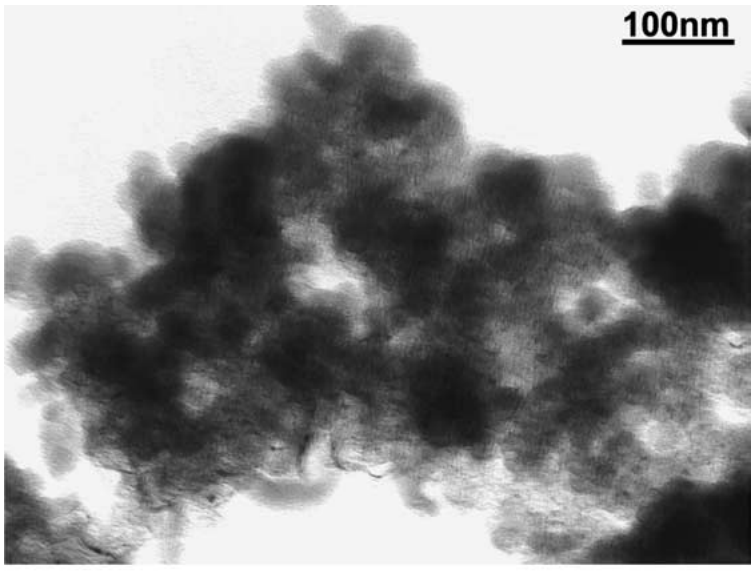

(c)

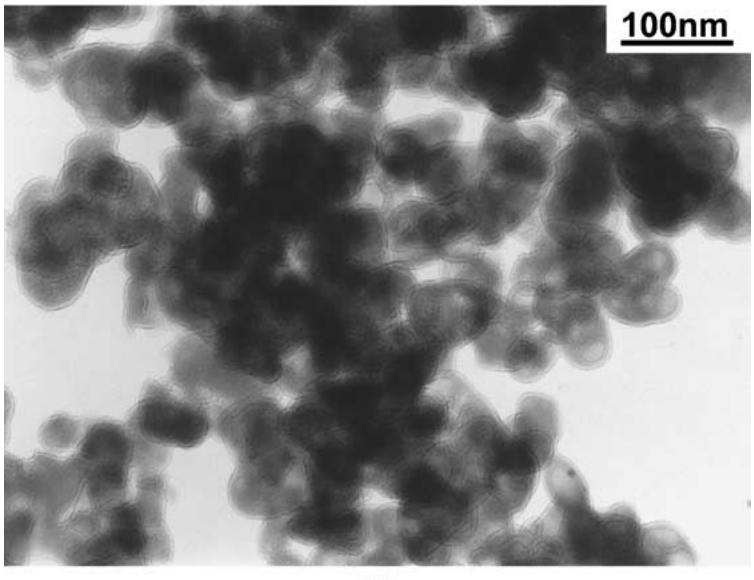

(d)

Figure 3 (*Continued*)

uniaxially compacted at 500 MPa into beams with the dimensions of 5 × 5 × 36 mm. The green beams were sintered at 1200–1300°C for 2 h and then polished with 6 μm diamond paste before testing.

2.3. Characterisation

The phase composition of the 'as prepared' and calcined composite powders were analysed by X-ray diffraction (XRD) using a Bruker AXS, D8 Advance Diffractometer with Cu K_α radiation at 40 kv and 40 mA. Data were collected over the 2θ range from 10 to 60° at a step size of 0.02° and a step time of 0.5 s.

The particle morphology of the 'as prepared' and calcined composite precipitates was observed using a transmission electron microscope (TEM) (JEM 100CX, Jeol, Japan). The water suspensions of sample powders were first ultrasonicated and then placed on copper grid covered with carbon film for the TEM observation.

The morphology of the polished and fractured surfaces of the sintered beams was observed on a field emission gun scanning electron microscope (FEGSEM) (LEO 1530 VP, United Kingdom). The fracture surface of bending tests were directly observed, while the polished surface was etched with 0.05 M hydrochloric acid before observation.

Energy dispersive analysis of X-ray (EDAX) was also conducted on the same FEGSEM for the semi-quantitative evaluation of the chemical compositions of sintered beam surfaces. Data acquisition was performed at 20 kv for 100 s on the gold-coated surfaces. Both etched and un-etched surfaces were evaluated.

3. Results and discussion

3.1. Morphology of the composite nanoparticles and the sintered composites

The typical micrographs of the 'as prepared' composite precipitates were shown in Figs 1 and 2. It can be

seen that they are nano-sized particles, but the particle morphology is entirely different from their neat components. The corresponding pure Al_2O_3 precursor precipitates are roughly spherical nanoparticles, while the pure TCP precipitates are needle-like nanoparticles with large length-to-width aspect ratio and are also highly agglomerated. In addition, the particle morphology of the composite precipitates also changes with synthetic parameters, such as Ca/P ratio and pH condition.

For the composite precipitates synthesised in neutral condition (pH = 7.0), the composite precipitates show irregular but elongated shape at lower Ca/P ratios. These particles interconnect to form a network-like morphology. The individual TCP or Al_2O_3 precursor particle is hardly distinguishable in this TEM micrograph (Fig. 1 top). However, more roughly spherical particles, which are well distributed in the precipitates, are observed with increasing Ca/P ratio (Fig. 1 middle and bottom). These nano-sized spheres are considered to be Al_2O_3 precursor particles based on the morphology of the neat components. The EDAX analysis shows that calcium, aluminium and phosphorus elements are present in each of the composite nanoparticles, suggesting that the two components mixing at very small scale. However, the high aggregation of these nanoparticles and the sharpness limitation of electronic beam restrict the resolution of EDAX analysis. Some other particles closely surrounding the single nanoparticle under analysis may also be covered in the EDAX results.

For the composite precipitates synthesised in alkaline condition (pH = 9.2), higher Ca/P ratios lead to the increase in particle size. However, less individual particles are distinguishable as well at higher Ca/P ratios (Fig. 2). This trend of morphology change with Ca/P ratio is opposite to that coprecipitated at pH 7.0. It may relate to the different phases formed at different pH conditions. The phase structure of the composite nanoparticles is discussed in the next section of this paper.

Fig. 3 shows the particle size and morphology of the calcined composite coprecipitates and the

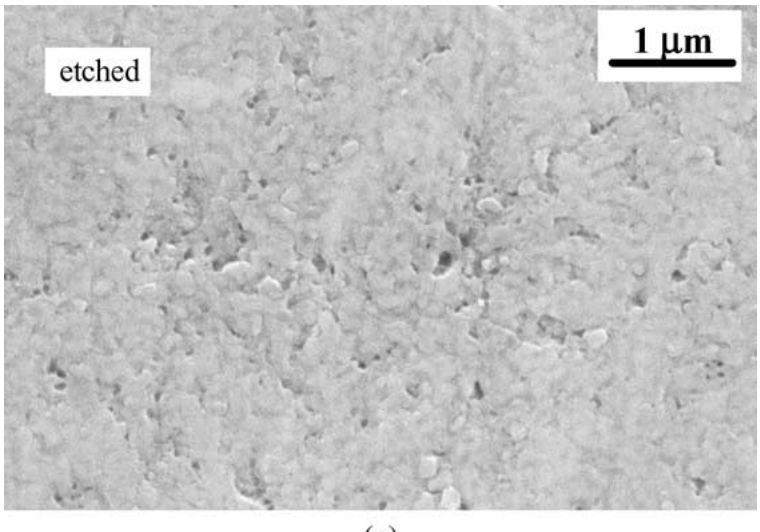

(a)

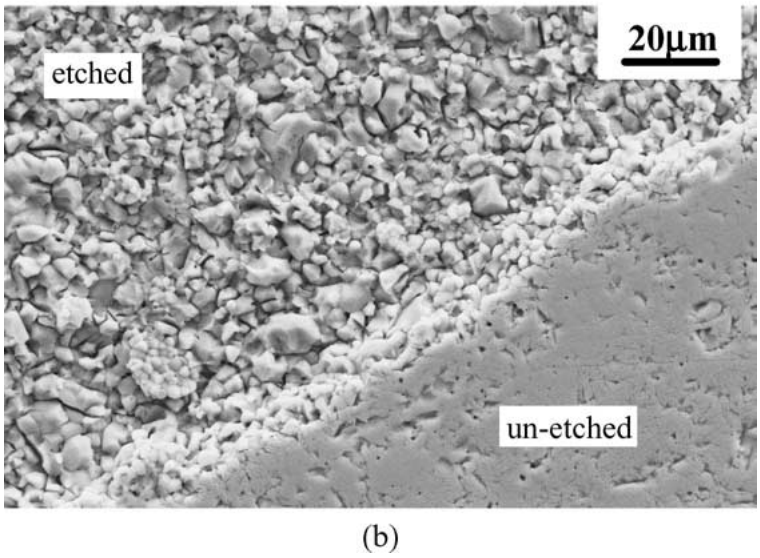

(b)

Figure 4 The FEGSEM micrographs for the compacts of neat components and composites containing 40 wt% Al_2O_3 after sintering at 1200°C for 6 h. Both etched and un-etched surface are shown in the micrographs: (a) neat Al_2O_3, (b) neat TCP, (c) nanocomposite prepared at pH = 7.0, and (d) nanocomposite prepared at pH = 9.2. (*Continued*)

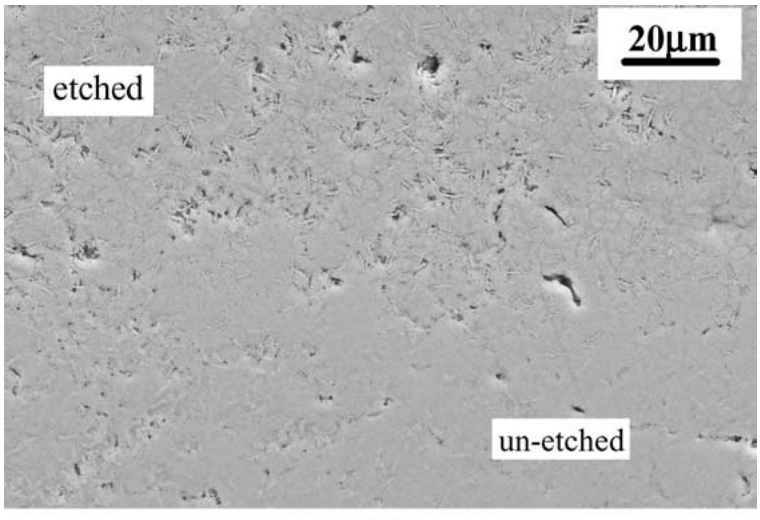

(c)

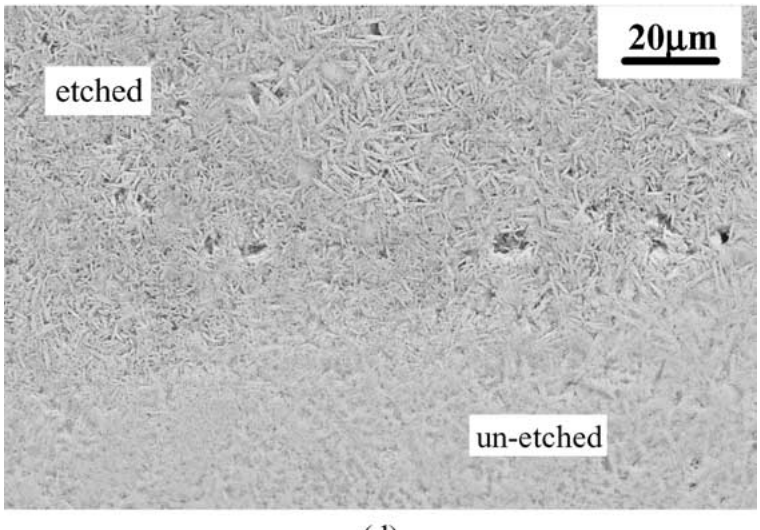

(d)

Figure 4 (*Continued*)

corresponding neat component precipitates. The particle size and morphology change a great deal, comparing with the 'as prepared' ones. The neat Al_2O_3 precipitates retain as nanoparticles (ca. 20 nm) after calcination, whereas the neat TCP precipitates increase to micron-scale (ca. 1 μm). The particle sizes of composite precipitates, however, are still in nano-scale (less than 100 nm), though they are larger than neat Al_2O_3 particles, but much smaller than TCP particles. In consideration of that the TCP is the major phase in these composite samples, it is clear that the existence of Al_2O_3 restricts the coarsening of TCP particles during calcination.

In addition to particle size, the distinct difference in particle morphology are also reflected in Fig. 3. The particle morphology difference between 'as prepared' and calcined samples can be expected because they undergo dehydration and coarsening during calcination. It is also easy to explain the difference between neat component and composite particles since they are different materials. However, it is interesting to find that the morphologies differ from each other for the composite nanoparticles coprecipitated under neutral or alkaline conditions. Under neutral coprecipitation condition, the highly agglomerated composite nanoparticles with large size distribution are produced after calcination, and the two components are not distinguishable in the TEM image. On the other hand, for the composite nanoparticles coprecipitated under alkaline condition, the calcined nanoparticles are well distinguishable in roughly spherical shape with more uniform size distribution and show somewhat core-shell structure. These micrographs confirm that the coprecipitated composite nanoparticles form uniform nanocomposites after calcination, in spite of their different morphologies. Similar results are obtained for the nanocomposites with different Ca/P molar ratios.

Fig. 4 shows the morphology of compacts after sintering. The grain morphology is quite different for the neat component materials and composites. The sintered neat Al_2O_3 compact consists of great number of small grains in submicron sizes, while the neat TCP compact comprises angular grains with the sizes of several microns. The composite compacts, however, contain some fibrils with the length of ca. 8 microns and an aspect ratio about 10. In addition, much more fibrils were observed in the sintered compacts synthesised at pH 9.2 than that

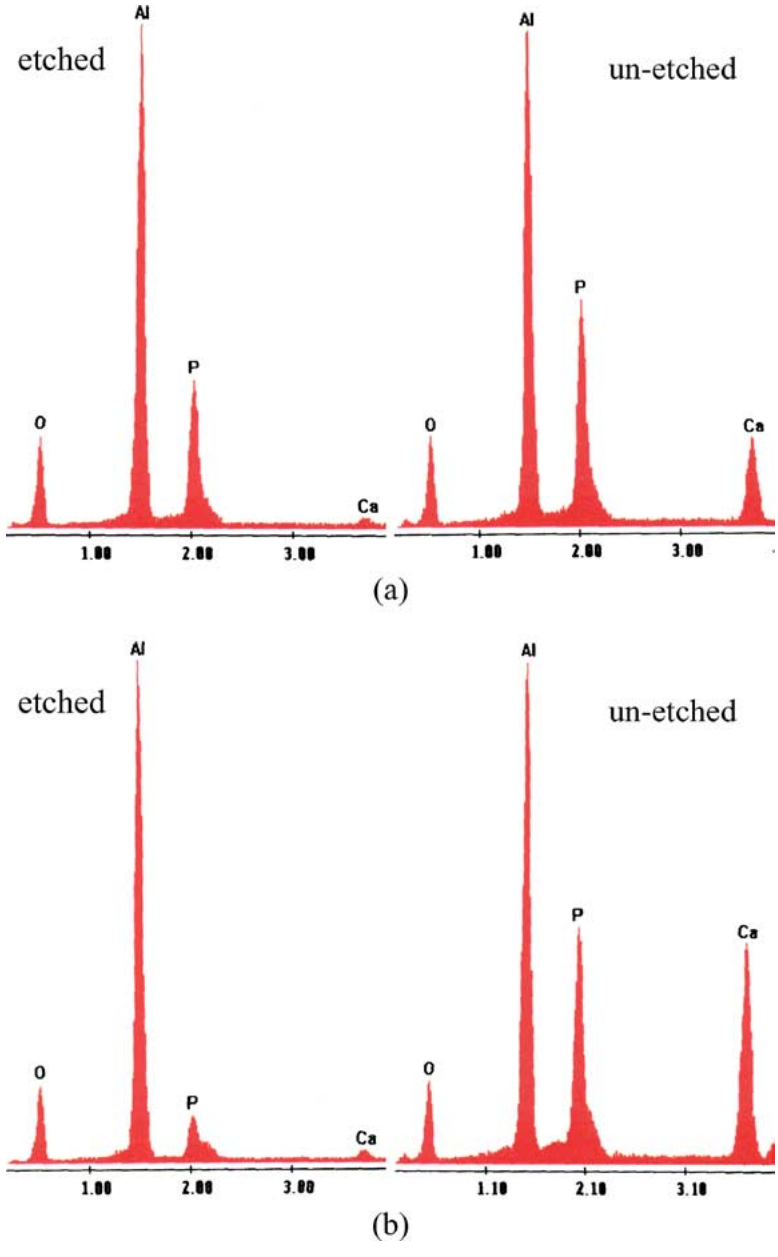

Figure 5 EDAX analyses of general area scanning for the TCP/Al_2O_3 = 60/40 compacts on the etched and un-etched surfaces: (a) nanocomposite prepared at pH = 7.0 and (b) nanocomposite prepared at pH = 9.2.

at pH 7.0. This is clearly shown in the etched parts of micrographs (c) and (d) in Fig. 4. Since the diluted hydrochloric acid (0.05N) cannot etch alumina at room temperature, it is believed that the fibrillar phase is alumina or at least in rich of alumina. The EDAX analyses on the polished and etched surfaces support this consideration. As shown in Fig. 5, the etched surfaces contain less phosphorus and calcium elements compared with un-etched ones, while the etched surfaces clearly show the fibrils in the composites. This is the first time to observe that a fibrillar alumina phase is *in situ* produced in the TCP/Al_2O_3 composites, which forms the basis for fabricating self-reinforcing composites.

3.2. Phase composition of the composite nanoparticles and sintered composites

The XRD analyses were carried out in order to characterise the phase structure of the calcined composite nanoparticles. Results show that both β-TCP and α-Al_2O_3 are present in the composite nanoparticles after calcinations. The phase composition, however, changes a great deal with the pH condition of precipitation media as well. Results of the influence of precipitation medium pH value on the calcination behaviour and phase composition are shown in Fig. 6. For the composite nanoparticles prepared in neutral condition (Fig. 6a), no crystalline phase is detected after calcination at 800°C for 6 h. The diffraction peaks for β-TCP [6] are only observed at 1000°C and the strongest diffraction peak is at $2\theta = 21.54°$. For the precursors coprecipitated at alkaline condition (Fig. 6b), however, diffraction peaks are detectable at 800°C and the strongest diffraction peak is at $2\theta = 31.08°$. These different behaviours of calcination result from the different chemical structures of the precursors and the calcined products, which are reflected by the difference in the strongest diffraction peaks of the calcined composite nanoparticles prepared under the two pH conditions. On the other hand, the α-Al_2O_3 phase [18] can only be

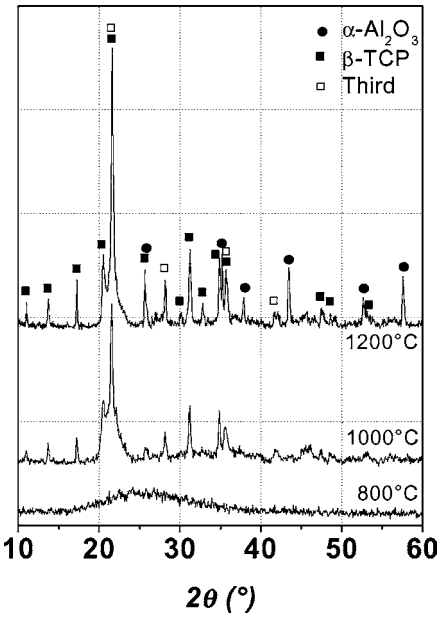

(a)

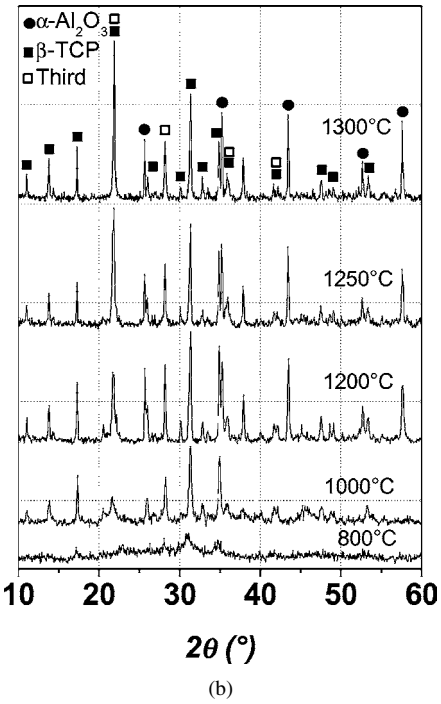

(b)

Figure 6 The XRD spectra for the TCP/Al_2O_3 = 60/40 composite nanoparticles calcined at different temperatures for 6 h and synthesised under: (a) pH = 7.0 and (b) pH = 9.2.

detected after calcination at 1200°C for both pH conditions of precipitation.

There are two principal phases, β-TCP and α-Al_2O_3, and a third minor phase in the composite nanoparticles as assigned on the spectra in Fig. 6. However, the phase compositions of the composite nanoparticles are strongly dependent on the pH condition of simultaneous precipitation. The major phases in the composite nanoparticles coprecipitated at pH 9.2 are β-TCP and α-Al_2O_3 after calcination, with the minor phase mainly being calcium aluminates [19] and calcium aluminium phosphates [20] (Fig. 6b). On the other hand, the minor phase increased remarkably in the composite nanoparticles coprecipitated at neutral condition (Fig. 6a), as indicated by the diffraction peak at $2\theta = 21.54°$, which is assigned as aluminium phosphate ($AlPO_4$) [21] and some other calcium phosphates such as $Ca(P_4O_{11})$ [22], though the accurate identification is difficult because of overlapping of the diffraction peaks. It is clear, however, that the formation of β-TCP strongly depends on the pH of precipitation media. These results are in consistence with the FEGSEM observations (Fig. 4c and d), where much less α-Al_2O_3 fibrils exist in the composite nanoparticles synthesised at pH 7.0 compared with those synthesised at pH 9.2. It is believed that the formation of $AlPO_4$ consumes a portion of aluminium resource, leading to less production of α-Al_2O_3 phase in the sintered composites.

Fig. 7 shows the XRD spectra of the composite nanoparticles with various Ca/P ratios. All of the spectra are similar for the composite nanoparticles synthesised at the same pH condition, indicating that the change of phase composition with Ca/P molar ratio is not so sensitive as to pH value. However, the relative amount of each phase in the composite nanoparticles does change with Ca/P ratio, especially for α-Al_2O_3phase. This can be shown by comparing the intensities of characteristic diffraction peak for each phase in the same spectrum, e.g., the peak height ratio of phosphate to alumina. Since the two peaks under comparison are chosen from the same XRD spectrum, the peak height ratio must reflect the amount ratio of each phase in the composite nanoparticles. The results are plotted in Fig. 8, where the height ratio of phosphate phase ($2\theta = 21.54°$ for pH 7.0 and $2\theta = 31.08°$ for pH 9.2) to that of alumina ($2\theta = 43.44°$) are shown as a function of Ca/P ratios. The peak height ratio decreases slightly with the increase of Ca/P ratio for the pH 7 series of composite nanoparticles, indicating a slight increase of α-Al_2O_3 phase in the final composite nanoparticles. On the other hand, the peak height ratio of β-TCP to α-Al_2O_3 increases with increasing the Ca/P ratio for the pH 9.2 series of composite nanoparticles, implying the reduced relative amount of α-Al_2O_3 phase in the composite nanoparticles. As mentioned above, the relative peak height can be taken as a semi-quantitative measure of the corresponding phase in the composite nanoparticles. That is, under alkaline condition less α-Al_2O_3 phase is formed in high Ca/P ratio composite nanoparticles. This may be due to the excess of calcium leads to formation of calcium aluminates [19]. While in neutral reaction condition, a slight more α-Al_2O_3 phase is present in high Ca/P ratio composite nanoparticles. This may result from the excess of calcium suppressed $AlPO_4$ formation, so that less aluminium is consumed for the formation of $AlPO_4$.

The pH 9.2 series of composite nanoparticles with different composition ratios and the corresponding sintered sample beams, which are used for mechanical measurements, are also analysed by the XRD measurements, and the results are shown in Fig. 9. No difference was observed in the XRD spectra, whatever the samples were in the form of composite nanoparticles or sintered compact beams. There are only β-TCP diffraction peaks detected in the spectra when its content is high

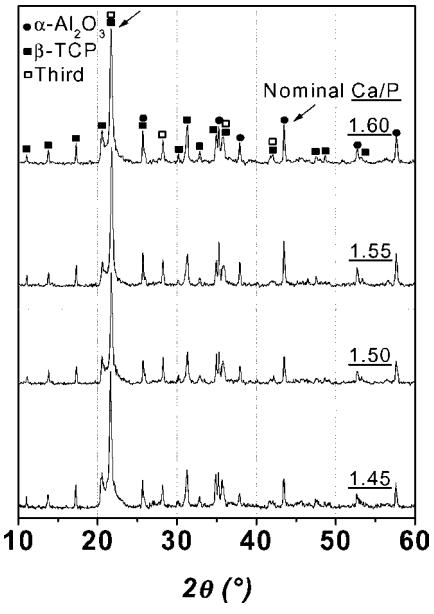

(a)

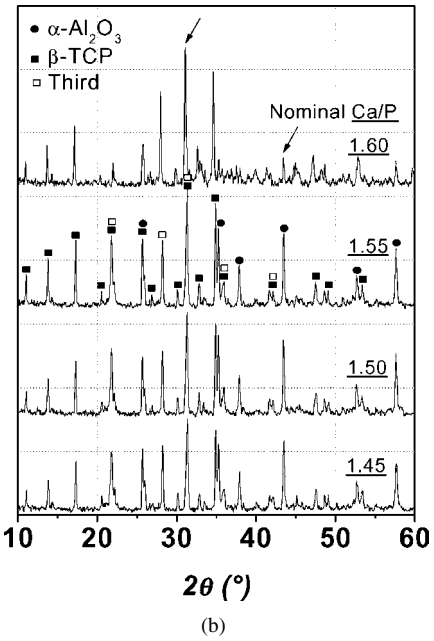

(b)

Figure 7 The XRD spectra for the TCP/Al_2O_3 = 60/40 composite nanoparticles with various Ca/P ratios after calcination at 1200°C for 6 h and synthesised under: (a) pH = 7.0 and (b) pH = 9.2.

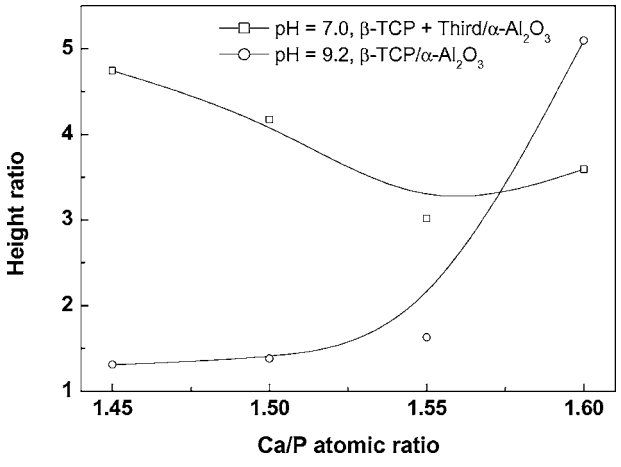

Figure 8 Height ratios of the characteristic diffraction peaks of β-TCP (2θ = 31.08°) or β-TCP plus $AlPO_4$ (21.54°) to α-Al_2O_3 (43.44°) as a function of Ca/P ratios for the composite nanoparticles synthesised under different pH conditions.

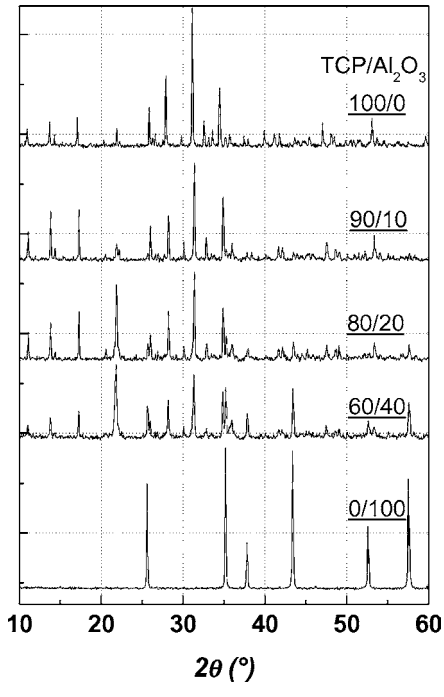

Figure 9 XRD spectra for the composite compacts with various composition ratios after sintering at 1250°C for 2 h.

(say 90 wt%), while α-Al_2O_3 phase is not detectable. As the increase of alumina content to 20 wt% or higher, the diffraction peaks characteristic of α-Al_2O_3 phase are clearly shown in the spectra, accompanying by the decrease in intensities of β-TCP diffraction peaks. This trend is consistent with the result shown in Fig. 7b, where the high Ca/P ratio leads to less α-Al_2O_3 formation in the nanocomposites. The loss of α-Al_2O_3 phase is due to the solid reaction between TCP and Al_2O_3 leading to form calcium aluminates. Ji and Marquis [18] have reported the similar result for the composite containing 80% hydroxyapatite and 20% Al_2O_3. No α-Al_2O_3 phase was detected in their composite after sintering at 1200°C. In our case, the solid reaction must be easier because the TCP and Al_2O_3 were simultaneously precipitated which led to better mixing up of the two components.

3.3. Mechanical strength of the sintered composites

Fig. 10 shows the mechanical property of the composites with various compositions after sintering at various temperatures. It is seen that both composition and sintering temperature have striking effects on the mechanical strength. The highest strengths are obtained for all the composites sintered at 1250°C with α-Al_2O_3 up to 40 wt%. When sintering at 1200°C, the composites with higher α-Al_2O_3 fractions have lower strengths than those sintered at 1250 and 1300°C, which is because the Al_2O_3 phase is not completely sintered at this temperature. Actually, it was found that the neat Al_2O_3 compacts sintered at these temperatures have almost no strength and the flexural strength of 204 MPa was obtained when sintering at as high as 1560°C. The above results indicated that the sintering temperature of

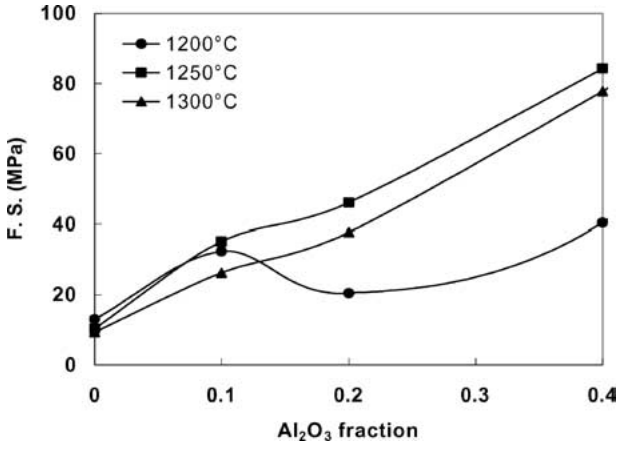

Figure 10 The flexural strength of composites prepared at pH 9.2 as a function of compositions and sintering temperatures.

Al_2O_3 phase is lowered in the composites. It is interesting, however, to notice that the composite strengths are lower when sintering at 1300°C than at 1250°C for all the compositions. This probably because the higher extent of decomposition at 1300°C leads to the strength decrease of the sintered composites, as the XRD (Fig. 6b) shows that the relative height of diffraction peak at 21.86° which assigns to (024) plane of β-TCP crystal and overlaps with the (111) plane diffraction of $AlPO_4$ crystal [21], has increased obviously. In addition, the small peak at 20.20° assigning to (202) plane of β-TCP crystal has disappeared.

The flexural strengths of sintered composites increase with α-Al_2O_3 fractions almost linearly, and reach to 84 MPa at the α-Al_2O_3 fraction of 0.4, indicating obvious effect of reinforcement. As shown in Fig. 10, even 10 wt% α-Al_2O_3 can result in 230% increase in flexural strength compared with neat β-TCP. The flexural fractures of the composites are displayed in Fig. 11. The grains sizes of composites are between the two neat components and change toward to α-Al_2O_3 as its fraction increasing. Furthermore, the grain interfaces are not as sharp as the neat component materials, suggesting the good bonding between the two phases.

As a result, it is believed that the remarkable reinforcing effect of α-Al_2O_3 results from its *in situ* formed

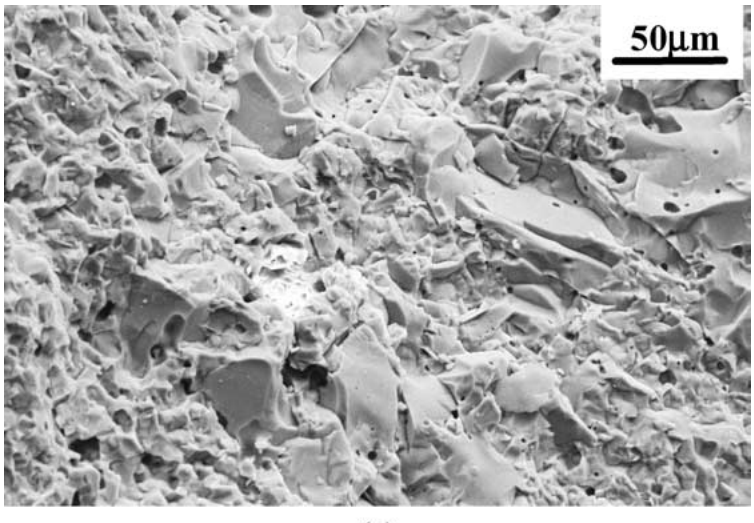

(a)

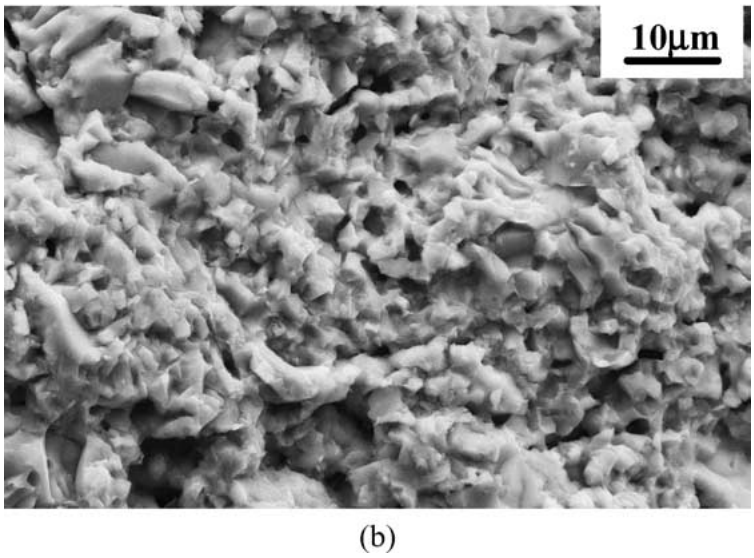

(b)

Figure 11 The morphology of flexural fractures of the neat components and composites prepared at pH 9.2 and sintered at 1250°C for 2 h: (a) neat β-TCP (note the scale bar differed from that in other micrographs), (b) composite with 10 wt% α-Al_2O_3, (c) composite with 40 wt% α-Al_2O_3, and (d) neat α-Al_2O_3. (*Continued*)

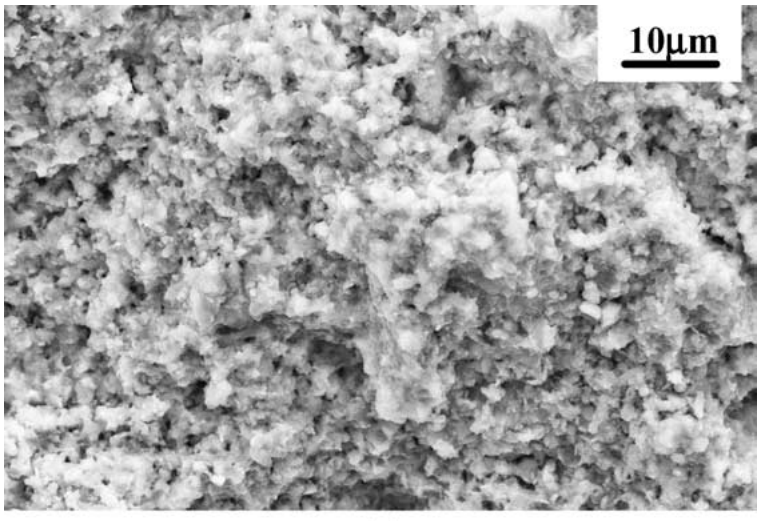

(c)

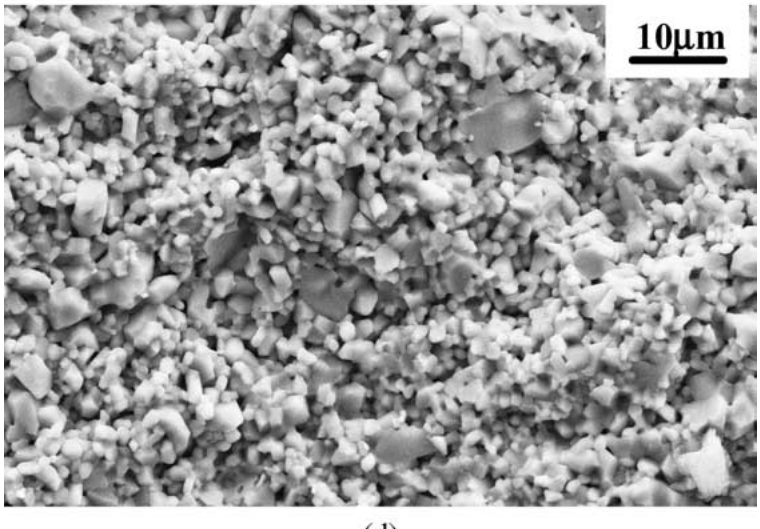

(d)

Figure 11 (*Continued*)

fibrillar phase structure and its distinct role of reducing grain dimensions.

4. Conclusions

The simultaneous precipitation of aqueous solutions of $CaCl_2$, $AlCl_3$ and $(NH_4)_2HPO_4$ by addition of NH_4OH solution produces composite nanoparticles consisting of β-TCP, α-Al_2O_3 and a small amount of the third minor phase. The minor phase, mainly $AlPO_4$, increases a great deal when simultaneously precipitated at pH 7.0 compared with pH 9.2.

The composite precipitates are nano-sized particles which interconnect into a network-like morphology, but the individual TCP or Al_2O_3 particles are hardly distinguishable in the composite precipitates. Calcination at elevated temperature converts the composite precipitates into nanoparticles which show somewhat core-shell structure.

The calcination behaviour of the composite precipitates and the phase composition of the resulting composite nanoparticles are strongly dependent on the pH of precipitation media. The composite precipitates prepared at pH 7.0 crystallise at 1000°C, whereas those prepared at pH 9.2 do at 800°C.

The Ca/P molar ratio shows no obvious effect on the phase structure of the composite nanoparticles. However, higher Ca/P ratio suppresses the formation of α-Al_2O_3 in the composite nanoparticles prepared pH 9.2.

Sintering of composite compacts at elevated temperature leads to formation of the self-reinforcing composites where the α-Al_2O_3 phase is in fibrillar form dispersed in the phosphate phases, imparting the unique role of self-reinforcement. Alkaline precipitation condition produces much more α-Al_2O_3 fibrils than neutral precipitation condition do.

The flexural strengths of the composites increase with increasing alumina fraction and are about 8 times as high as neat β-TCP at the α-Al_2O_3 fraction of 0.4. The highest flexural strengths are obtained when sintering at 1250°C for 2 h.

Acknowledgements

The authors would like to show their sincere thanks to the EPSRC for the financial support of this research. Special acknowledgement gives to Dr. D. H. Ross for his kind help and invaluable advice in XRD measurements.

References

1. I. MANJUBALA and M. SIVAKUMAR, *Mater. Chem. Phys.* **71** (2001) 272.
2. K. THOMA, R. ALEX and E. FENSCHKLEEMANN, *Euro. J. Pharm. Biopharm.* **38** (1992) 101.
3. A. AKASHI, Y. MATSUYA, M. UNEMORI and A. AKAMINE, *Biomaterials* **22** (2001) 2713.
4. A. CUNEYT TAS, F. KORKUSUZ, M. TIMUCIN and N. AKKAS, *J. Mater. Sci., Mater. Med.* **8** (1997) 91.
5. F. KORKUSUZ, A. UCHIDA, Y. SHITO, N. ARAKI, K. INOUE and K. ONO, *J. Bone Joint Surg.* **75-B** (1993) 111.
6. A. ITO, K. OJIMA, H. NAITO, N. ICHINOSE and T. TATEISHI, *J. Biomed. Mater. Res.* **50** (2000) 178.
7. J. M. BOULER, R. Z. LEGEROS and G. DACULSI, *ibid.* **50/51** (2000) 680.
8. A. SLOSARCZYK and J. PIEKARCZYK, *Ceram. Intern.* **25** (1999) 561.
9. X. H. YANG and Z. H. WANG, *J. Mater. Chem.* **8** (1998) 2233.
10. E. ADOLFSSON, P. ALBERIUS-HENNING and L. HERMANSSON, *J. Amer. Ceram. Soc.* **83** (2000) 2798.
11. H. Y. JUANG and M. H. HON, *Mater. Sci. Eng.* **C2** (1994) 77.
12. E. ADOLFSSON, M. NYGREN and L. HERMANSSON, *J. Amer. Ceram. Soc.* **82** (1999) 2909.
13. K. S. OH, F. CAROFF, R. FAMERY, M. F. SIGOT-LUIZARD and P. BOCH, *J. Euro. Ceram. Soc.* **18** (1998) 1931.
14. T. KASUGA, M. SAWADA, M. NOGAMI and Y. ABE, *Biomaterials* **20** (1999) 1415.
15. K. YAMASHITA, E. YONEHARA, X. F. DING, M. NAGAI, T. UMEGAKI and M. MATSUDA, *J. Biomed. Mater. Res.* **43** (1998) 46.
16. Y.-K. JUN, W. H. KIM, O.-K. KWEON and S.-H. HONG, *Biomaterials* **24** (2003) 3731.
17. S. F. HULBERT, J. S. MORRISON and J. J. KLAWITTER, *J. Biomed. Mater. Res.* **6** (1972) 347.
18. K. T. HWANG, H. S. LEE, S. H. LEE, K. C. CHUNG, S. S. PARK and J. H. LEE, *J. Euro. Ceram. Soc.* **21** (2001) 375.
19. H. X. JI and P. M. MARQUIS, *J. Mater. Sci.* **28** (1993) 1941.
20. 2000 JCPDS-International Centre for Diffraction Data, PCPDFWIN v. 2.1 file No. 48-1192.
21. 2000 JCPDS-International Centre for Diffraction Data, PCPDFWIN v. 2.1 file No. 72-1161.
22. 2000 JCPDS-International Centre for Diffraction Data, PCPDFWIN v. 2.1 file No. 82-0902.

Received 28 February 2003
and accepted 3 June 2004